

Experimental analysis on the exploding wire process for nanopowder production: Influence of initial energy and exploding atmosphere

Gianluca Caposciutti¹, Bernardo Tellini¹, Paola Saccomandi², Alfredo Cigada²

¹ Department of Energy, Systems, Territory and Construction Engineering, University of Pisa, Italy

² Department of Mechanical Engineering, Politecnico di Milano, Italy

ABSTRACT

Metallic nanopowder is employed in several applications for its flexibility of use, thus its production is growing over the years. Exploding wire technique can produce a wide range of nanoparticles from electrically conducting samples, and it has a potential for high efficiency and productivity, due to the strongly localized power dissipation. On the other hand, the phenomena involved during the explosion are complex, and phenomenological relationships are usually considered for controlling the output product characteristics. In this study, we investigated the effect of the input energy and the medium in which the explosion takes place on the final dimensional distribution of the nanopowder. Utilizing a proper power supply and an exploding system developed on purpose, we applied up to 10 GA/m² to copper wire samples immersed in air or water. We collected the products for morphological analysis, we carried out a shape and dimensional characterization based on a statistical analysis of the obtained particles, and we compared and discussed the results concerning the adopted initial conditions and the most recent literature data.

Section: RESEARCH PAPER

Keywords: Nanopowder; exploding wire; nanoparticle distribution; morphology analysis

Citation: Gianluca Caposciutti, Bernardo Tellini, Paola Saccomandi, Alfredo Cigada, Experimental analysis on the exploding wire process for nanopowder production: Influence of initial energy and exploding atmosphere, Acta IMEKO, vol. 12, no. 2, article 29, June 2023, identifier: IMEKO-ACTA-12 (2023)-02-29

Section Editor: Andrea Scorza, Università Degli Studi Roma Tre, Italy, Roberto Montanini, Università degli Studi di Messina, Italy

Received December 5, 2022; **In final form** June 18, 2023; **Published** June 2023

Copyright: This is an open-access article distributed under the terms of the Creative Commons Attribution 3.0 License, which permits unrestricted use, distribution, and reproduction in any medium, provided the original author and source are credited.

Corresponding author: Gianluca Caposciutti, e-mail: gianluca.caposciutti@unipi.it

1. INTRODUCTION

Metallic-based nanoparticles are of great interest due to their versatility of use. Indeed, they can be deposited over or embedded into support materials to vary the overall physical and chemical properties. For instance, nanoparticles are used as surface coating agents to control the surface electrical and thermal conductivity, to improve its mechanical resistance, to increase its performance against chemical agents, and to control its optical characteristics [1]–[3]. Moreover, nanoparticles can be used in combination with different substrates, such as polymers [4], thus controlling the mean properties of the resulting medium, and allowing the development of novel materials [5]. Therefore, nanoparticles find a wide application in several sectors, from nano-biomedicine to sensors and transducer manufacturing. Indeed, nanoparticles can be used to boost the sensing performance of several devices, such as environmental sensors

and bio-sensors [6]–[8], or the efficiency of batteries [9] among the others.

Nanoparticle morphology has a large impact on the resulting application effectiveness; indeed, equivalent diameter, shape, and chemical composition are of great relevance to this purpose. These values mainly vary as a function of the materials involved, and the production process itself. Literature describes several techniques for nanoparticle production. For instance, laser-growth allows depositing particles with a diameter in the order of the laser wavelength but results in several thermal issues which can affect the particle dimension control [10]. Moreover, the operation of lasers, both for growing or ablating-based techniques, can generate unwanted and/or toxic secondary products [11]. Mechanical methods, such as grinding and milling, can result in time-consuming or energy-expensive processes [12], [13]. Chemical deposition and similar bottom-up approaches allow the growth of metal nanoparticles with satisfactory control of their morphology; however, the main disadvantage lies in the

use of potentially hazardous and environmentally toxic chemicals, thus reducing the sustainability of this method [14].

Among the others, wire explosion is a promising technique [15] used to produce nanoparticles from wires based on conducting materials.

For this purpose, a current of magnitude $10^7 - 10^9 \text{ A/m}^2$ [16] flows throughout the sample, and a quick joule adiabatic heating and a further explosion produce a mixture of liquid-gas metal clusters and ionized plasma [17]-[18]. Therefore, the vapours undergo rapid nucleation to form the desired nanoparticles [17]. Concerning other strategies, the use of harmful chemicals is avoided, and the very localized power dissipation limits the process duration, reduces the thermal losses, and possibly enhances both energy efficiency and productivity [19]. Moreover, this method is flexible and can produce multicomponent nanostructures [18], even if immiscible with standard techniques [20].

The process behaviour depends on complex interactions among thermal, mechanical, and electromagnetic phenomena into play, and a consistent model of this process is still lacking in literature [20]. Therefore, a phenomenological approach is often pursued to study the relationship between the input process parameters and the resulting nanoparticle characteristics.

For instance, the exploding atmosphere has a large influence in terms of product chemistry, as showed in [21]-[22], but also affects the product nucleation behaviour and the final morphology. Moreover, exploding energy and timing are crucial to control the final dimensions of the nanoparticles [23].

In this work, we used a wire explosion technique to produce copper-based nanoparticles from a copper wire sample. We provide experimental results utilizing different current densities and different mediums in which the explosion takes place. Therefore, we characterized the morphology of the products by measuring and describing the granular distribution and the particle shape, thus investigating the relationship between the product characteristics, and the operating conditions employed.

2. EXPERIMENTAL SETUP

As an exploding sample, we used specimens made of 4 twisted 0.1 mm diameter copper wires having a length of 40 mm circa. The wires come from commercial electrical wiring (i.e., standard 16 A cable with a 4 mm² cross-section). We prepared a set of 30 samples, from which we randomly selected the ones for the tests (i.e., 2 samples per test case).

The outer diameter of the specimens resulted in about 0.4 mm, and their mass in about 0.14 g. We housed the wire between two aluminium electrodes with 3 mm thickness with dedicated screw connectors. The length of the electrodes, constant in the tests, determines the active length of the specimen (i.e., about 30 mm) which is the distance between the aluminium plates.

Therefore, we measured the resistance between the electrodes for each tested sample as $10 \pm 2 \text{ m}\Omega$. We utilized the same initial configuration for all the test, thus limiting the variability on the results due to the setup. We placed the sample and the electrodes inside a cylindrical Nylon vessel with a 100 mm internal diameter and 100 mm height. We used a holed Nylon cap fixed with stainless-steel screws to enclose the environment and to retain most of the produced powder within the vessel. We connected the electrodes to a power coaxial cable via custom electrical connectors. A calibrated Rogowski coil [24] is wrapped around

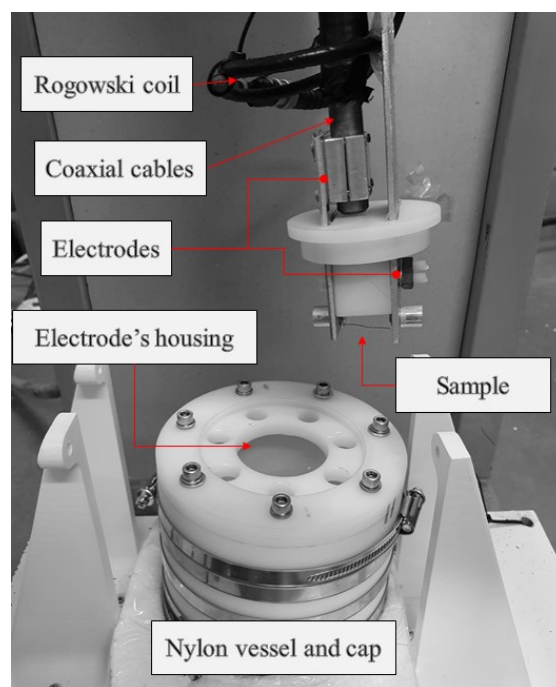


Figure 1. Picture of the explosion setup.

one electrode for current measurement purposes. Figure 1 shows the main components of the explosion setup.

The coaxial cable is connected to a power system made by a 765 μF capacitance, with a voltage limit of 10 kV. A high-voltage DC power supply allows to charge the capacitor to the desired voltage V , and an electronic control system allows a fast discharge thanks to an optical fiber trigger. We monitor the voltage using a 1:1000 dedicated probe. Depending on the system resulting impedance, we achieve a 10^{10} A/m^2 current density. The main contributions to the system inductance are the connections between the electrodes and the sample, the electrode geometry, and the plasma formed during the explosion process. Figure 2 shows a picture and the sketch of the power circuit.

We acquired signals from the Rogowski coil and the voltage probe by employing a Lecroy W wave Pro 725Zi (equipped with four 8-bit boards and 2.5 GHz bandwidth) and elaborated through a Matlab post-processing routine. When provided, the expanded uncertainties are calculated according to the GUM and with a coverage factor $k = 2$.

3. METHOD

3.1. Operating parameters

We provide a simplified scheme of the exploding wire process in the following paragraphs. First, a current flow passes through the sample, thus producing adiabatic heating due to the Joule effect. Indeed, the fast nature of the heating process (involving thousands of watts in tens of nanoseconds) does not allow a significant heat exchange with the surrounding medium. Therefore, the products (mainly vapours and ionized gas) rapidly expand while interacting with the explosion environment, thus nucleating and forming nanoparticles clusters. Generally, agglomeration occurs while the clusters are cooling down before their stabilization, thus producing macro clusters of nanoparticles. The initial energy, the flowing current, and the medium in which the explosion occurs have the main influence on the process behaviour. In particular, the initial energy E

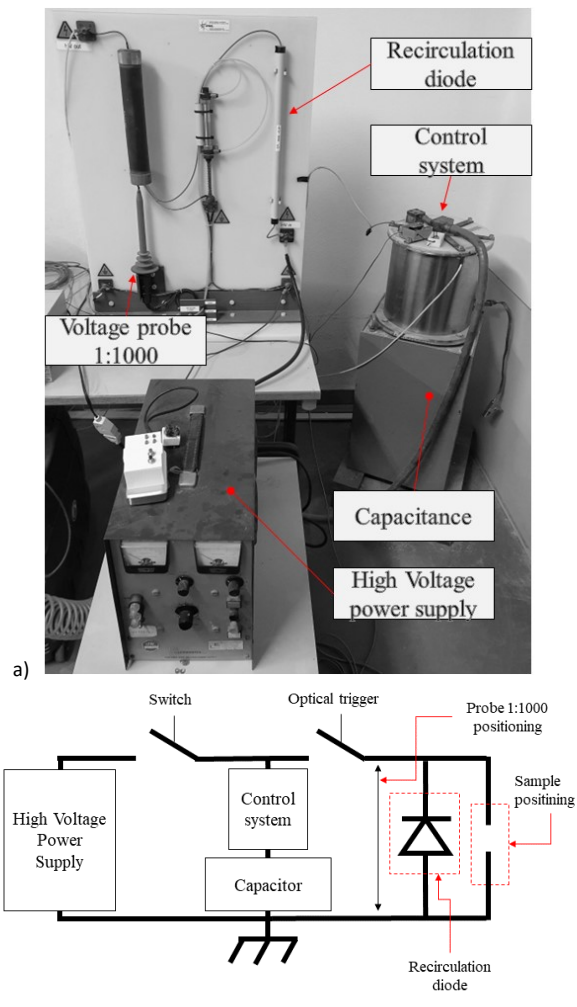


Figure 2. a) Picture and b) the scheme of the power circuit.

depends on the capacitor voltage V and capacitance C according to equation (1)

$$E = \frac{1}{2} C V^2 . \quad (1)$$

We set the initial capacitor voltage at 800 V, 1 kV, and 1.5 kV, hence we use an initial energy of 244 J, 382 J, and 860 J, respectively. By considering the system resistance R concentrated on the wire sample resistance R_s , the exploding power can be evaluated as a function of the circulating current I according to equation (2)

$$P = R_s I^2 . \quad (2)$$

The time behaviour of I depends on the inductance of the system, which is a function of the system geometry, of the involved materials, and of the plasma arc formed during the process. Apart from the stochastic nature of the plasma arc, the other impedance components are constant, and the current profile varies with the initial energy E .

As stated in [25], during the process onset the expansion rate is the highest, and ions are dispersed with kinetic energy proportional to E . Therefore, these ions are possibly responsible for nucleation centres. Moreover, the vapor supersaturation is high, hence condensation starts at the very beginning of the expansion and at the maximum rate.

Therefore, a higher E causes a larger ion dispersion, the nucleation occurs on a less dense areas, and smaller particle diameter can be obtained. The medium in which the explosion occurs has a key role in the cooling and nucleation process. In particular, we infer that a denser fluid with larger heat capacity and thermal conductivity should increase the cooling rate, promoting a faster stabilization of the clusters and mitigating the agglomeration phenomena. On the other hand, a denser fluid can increase the particle-to-fluid drag, leading to a comprehensive negative effect, due to reduced ion dispersion. For comparison, we produced nanoparticles with air and distilled water as mediums in the same initial energy conditions, and we studied the resulting dimensional characteristics of the produced nanoparticles. Both the air and the water are utilized with initial temperature of 25 °C (i.e., environmental temperature).

3.2. Collections of the samples

We collected samples generated in air and water to analyse the products with a Coxem EM-30 scanning electron microscope (SEM). The collected samples are deposited over a 10 mm x 10 mm ultra-smooth pure silicon sample. In the case of tests with air, the silicon sample is housed at the bottom of the nylon vessel and directly exposed to the exploding wire (Figure 3a). In the case of tests carried out in water, the copper wire is immersed in the medium. The explosion causes the products to disperse in water; therefore, we collect the liquid (Figure 3b), and further evaporate it while the silicon sample is immersed with a dedicated system consisting in a custom static oven. Its temperature control is operated by means of 3 Pt100 RTD sensors and a PID controller operated by a LabView software made on purpose. This system can keep the desired temperature setpoint within 2 °C.

During the evaporation of water, small particles can be carried out by the vapor thus altering the final measured dimensional distribution. On the other hand, the sedimentation allows the particles to stick together due to cohesion, thus forming larger clusters of nanoparticles and reducing their mobility. High evaporation rate and temperatures can promote internal recirculation of liquid and nanoparticles, limiting the sedimentation rate. However, a high evaporation rate can also reduce the drying time, increasing the productivity of the process. Therefore, we evaporated the water at 40 °C as a trade-off between the minimum temperature and the minimum time for drying completion. We remark that the optimization of this procedure is out of the purpose of the present study and that higher drying temperatures could be successfully employed but after a proper assessment of its impact on the final products.

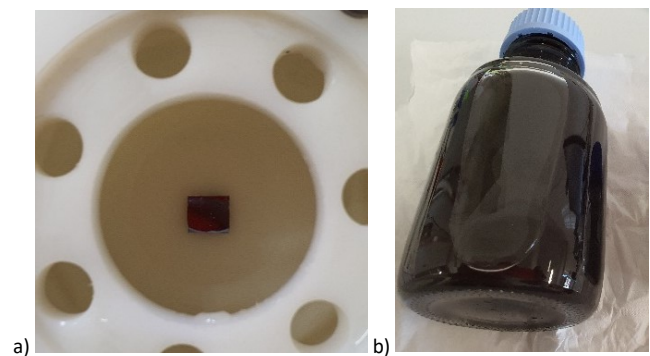


Figure 3. a) Sample positioning for the case of air as exploding medium and b) collected water sample during explosion in distilled water.

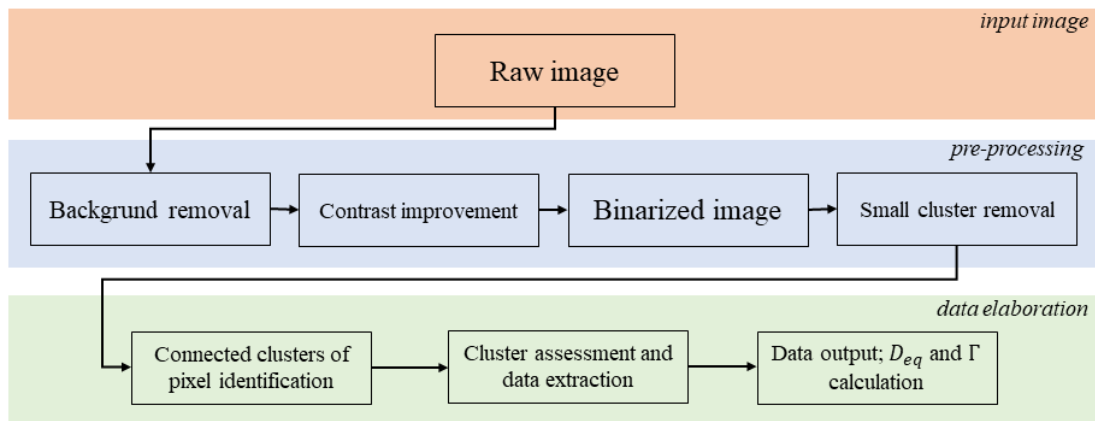


Figure 4. Scheme of the main steps involved in the image analysis process.

From the sample images, we expect to find particles ranging from tens to hundreds of nanometers. In order to carry out a statistical analysis on the product diameter, we require a significant number of samples per image. However, we restricted the measurement to the elements above 10 nm size, due to the reliability of both the measurement method and the SEM collected images. We found a satisfactory result using 5000× magnification during image acquisition.

3.3. Image analysis

We carried out image analysis utilizing a custom Matlab script. The SEM provide 8-bit grayscale images. The brightest pixel indicates the location of the nanoparticles, while the darkest pixel indicates the sample silicon background. First, we crop the image to the particles' area, and we filtered the pixel whose value is equal to or below the background one (i.e., background removal). Then, we increase the image contrast by exponentiating the pixel brightness values with a factor within 1.4 and 1.5 (i.e., contrast improvement), thus obtaining a steep gradient in the particle's proximity and located in a few pixels across the particles.

Therefore, we binarize the data utilizing a threshold based on the pixel brightness fixed at 30% of the maximum value. By varying this value from 20% to 40% we obtain a negligible influence on the results. Finally, we removed small or poorly connected pixel clusters by using the “bwareopen” function [26], and we use a routine based on the “regionprop” function [26] to get information from each isolated cluster. We considered each isolated cluster as a single particle, and the software provides the pixel area A_{px} and the perimeter p of each cluster. Therefore, we calculate the equivalent diameter D_{eq} and the circularity Γ as:

$$D_{eq} = 2 \sqrt{\frac{A_{px}}{\pi}}, \quad (3)$$

$$\Gamma = \frac{4 A_{px} \pi}{p^2}. \quad (4)$$

It is worth noting that $\Gamma = 1$ indicates a circular shape, while $\Gamma = 0$ possibly indicates elongated shapes or elements with jagged perimeter. Figure 4 shows a scheme of the main image processing steps.

Figure 5 shows a qualitative example of the algorithm operating steps.

The equivalent diameter measured by the aforementioned procedure is converted into S.I. units by means of the scale

provided by SEM images. For each single batch with the same operating condition, several images are analysed by the SEM analysis over different positions of the silicon sample, to maximize the statistical population (i.e., more than 600 particles are detected for each test). In particular, we were able to count 30 to 70 particles per image at 5k magnification.

According to the current literature [23], [27], [28], and as explained by the model used in [29], the particles produced via exploding wire recall a lognormal dimensional probability distribution. In this study, we assume the lognormal model to statistically describe the results, as suggested in literature. In particular, the lognormal distribution of D_{eq} is modelled as

$$\text{logn}(D_{eq}) = \frac{1}{D_{eq} \sigma \sqrt{2\pi}} e^{-\left(\frac{\ln(D_{eq}) - \mu}{2\sigma}\right)^2}. \quad (5)$$

The parameters μ and σ in (5) are calculated by fitting $\text{logn}(D_{eq})$ and D_{eq} ; therefore, the mean of D_{eq} with the lognormal distribution hypothesis (i.e., D_{eq}^*) can be calculated as [30]

$$D_{eq}^* = e^{\mu + \frac{\sigma^2}{2}}. \quad (6)$$

Moreover, we can calculate the fraction C of particles below a threshold diameter D_t , by using the cumulative distribution of $\text{logn}(D_{eq})$

$$C(D_t) = \int_0^{D_t} \text{logn}(x) dx. \quad (7)$$

Usually, nanoparticles are in the dimensional range of 10 to 100 nm. On the other hand, in some applications the size of the nanoparticles can reach up to 250 nm, as reported in [31]. Therefore, we use $D_t = 250$ nm to compute C for comparison purpose among the different operating conditions. Finally, we compare D_{eq}^* (obtained by considering a lognormal distribution) with the mean of the measured data D_{eq} .

4. RESULTS AND DISCUSSION

Figure 6 provides a comparison of the current profiles carried out from different test. Current data are calculated by integrating the voltage signal from the calibrated Rogowski coil. In particular, Figure 6a shows the comparison between air-based explosions at different initial voltage, and Figure 6b between air and water-based explosions at the same initial voltage.

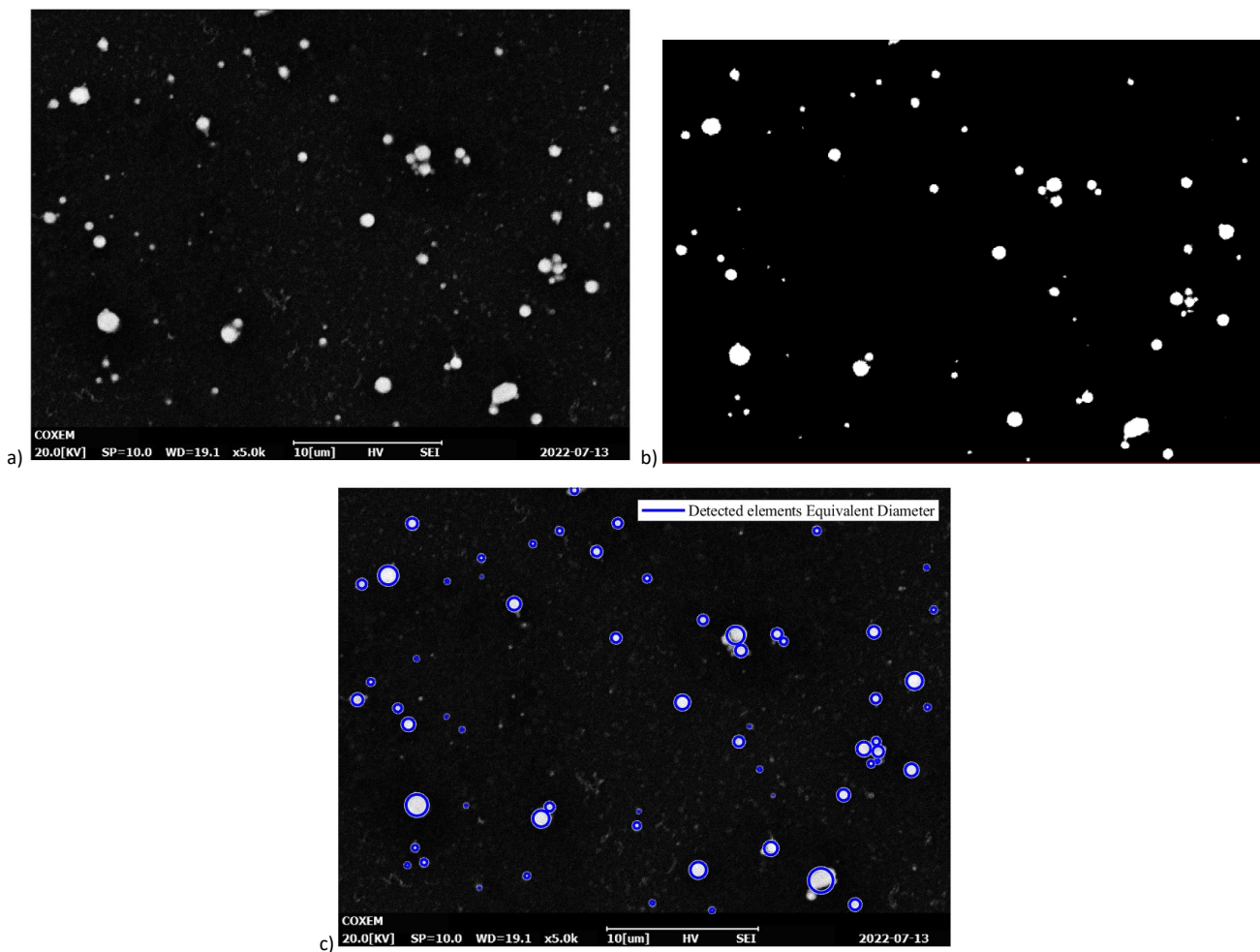


Figure 5. a) Original image, b) pre-processed image, and c) representation of the evaluated clusters equivalent diameter overlapped to the original image.

Figure 6b also shows a repeated test for the case of 1000 V – water medium, taken as example of test repeatability.

According to Figure 6a, the profile structure results in two different peaks at approximately 50 μs and 70 μs . This structure is consistent with literature results. For example, [32] reports that the first current drop is mostly due to the vaporization of the wire, which increases the resulting resistance. In a second phase, a plasma arc is formed, and the current starts to increase again

(i.e., the resistance decays) until the capacitor voltage supports the discharge process. The first peak time positioning delays when we adopt a lower initial voltage. Indeed, the lower injected energy leads to a slower current increase.

Figure 6b shows good accordance between repetitions made in the same operating conditions, despite small differences in the transient current profiles that can occur due to possibly small variations of the samples and capacitor initial voltage. As

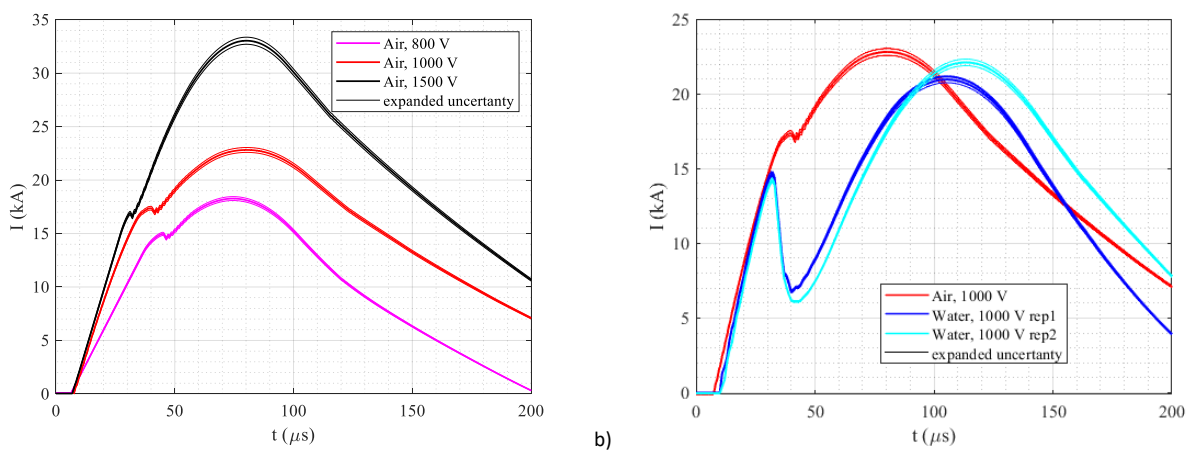


Figure 6. a) Comparison of the current profiles in case of air-based explosions at different initial voltage, and b) between different medium at the same input voltage i.e., rep1 and rep2 indicate the repetition of the same test. Small coloured lines report the expanded uncertainty for the measured current with a coverage factor $k = 2$.

expected, we obtained the same peak current of 23 kA by using the same input voltage. In the case of water, the first current peak anticipates, hence the wire explosion occurs at a lower current threshold. This fact depends on the complex exploding wire dynamic. We infer that the higher water density limits the initial expansion of the wire during the adiabatic heating process, thus increasing the sample's internal energy and allowing a quicker explosion behaviour. In the end, we calculate the maximum elapsed power at the first peak in the range between 2 to 3 kW.

In Figure 7 we report the qualitative results from the exploding wire process, highlighting the different powder sample large-scale differences concerning the exploding atmosphere and input energy.

From a qualitative analysis, the explosion atmosphere significantly affects the obtained result. Figure 7a and Figure 7b show particles with different shape; indeed, in the case of water the clusters borders are more jagged, and significantly more dispersed as well. This fact can be caused by the larger heat exchange possibly obtained in water, which induced cluster solidification before the surface tension allows the circular shape formation.

Figure 7c and Figure 7d suggest that high input energy can cause liquid particles to impact the silicon sample surface, possibly introducing a bias on the nanopowder sampling process. As per the case of droplets formation due to shock waves [33], the larger the inertial forces concerning the surface tension, the more cluster fragmentation is achieved, and we assume that the

higher the energy is released through the wire, the higher is the initial speed of the particles. Therefore, the high particle speed led to the impact of melted clusters on the silicon surface.

In Figure 8 we report the result of the statistical analysis on the particles in terms of equivalent diameter and circularity distribution concerning equations (3) and (4).

Figure 8a and Figure 8b suggest the particle distribution shift towards smaller D_{eq} when we utilize a higher initial voltage, independently by the exploding medium.

On the other hand, Figure 8c and Figure 8d show that the exploding medium has the larger influence on the particles shape, thus influencing the circularity of the particles. Indeed, the circularity for water-based explosion peaks at around 0.4, and the one for air-based explosion at around 0.7. On the other hand, E has a minor influence on Γ , affecting the circularity to a minor extent concerning the exploding medium. We use the data presented in Figure 8 to calculate D_{eq}^* and C as shown in Eqs. 6 and 7, thus obtaining a quantitative estimation of the dimensional characteristics of the products. The parameters associated with the obtained data are resumed and reported in Table 1.

Table 1 shows a satisfactory accordance between D_{eq}^* , calculated by considering a lognormal distribution of the equivalent diameter, and the mean of the data regarding the equivalent diameter D_{eq} .

In Figure 9 we report the behaviour of the lognormal distributions characteristics as a function of E .

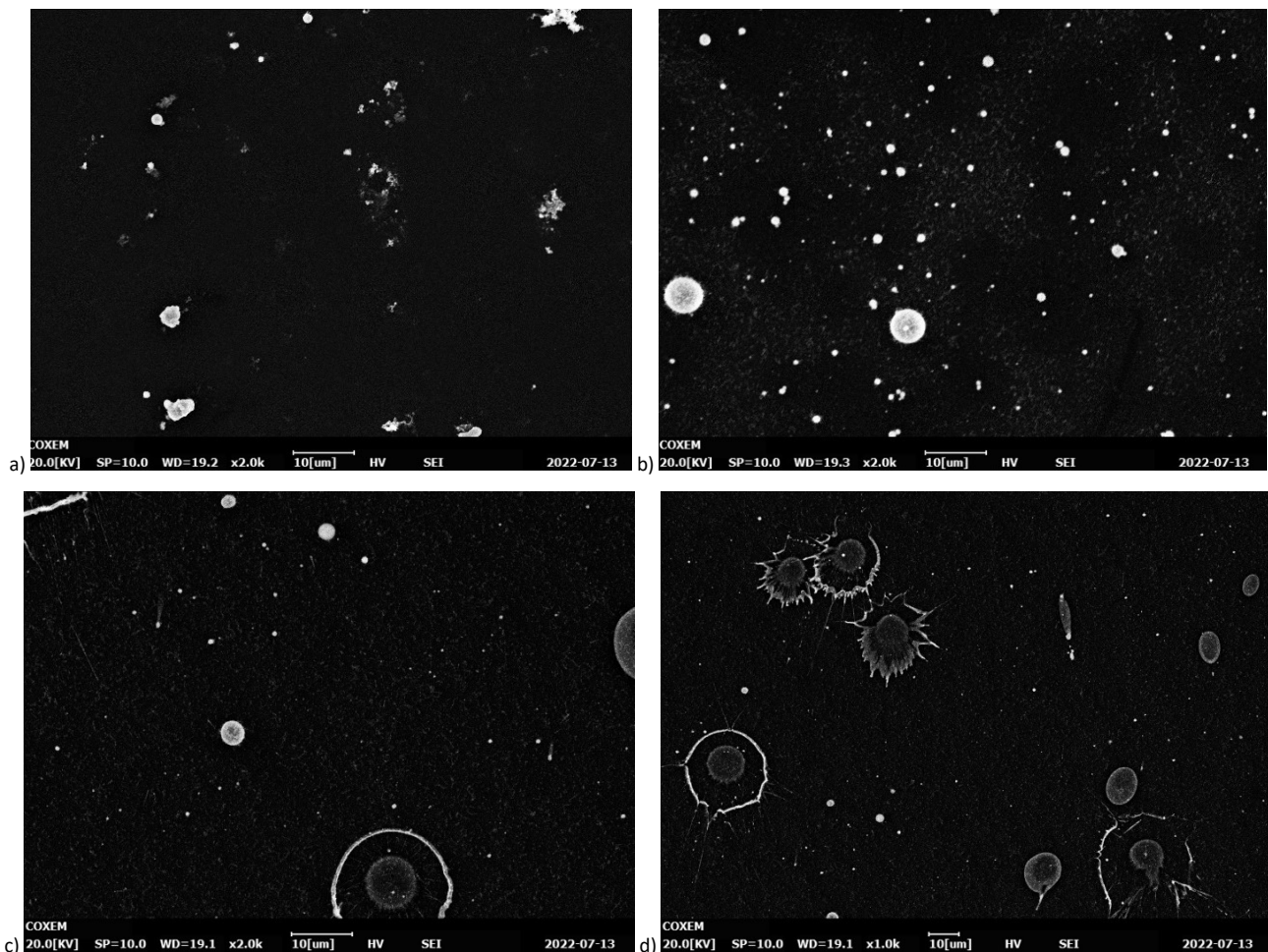


Figure 7. SEM images from samples with different exploding atmosphere and initial voltage: a) water 1 kV, b) air 1 kV, c) air 1.5 kV and 2000x magnification, and d) air 1.5 kV and 1000x magnification.

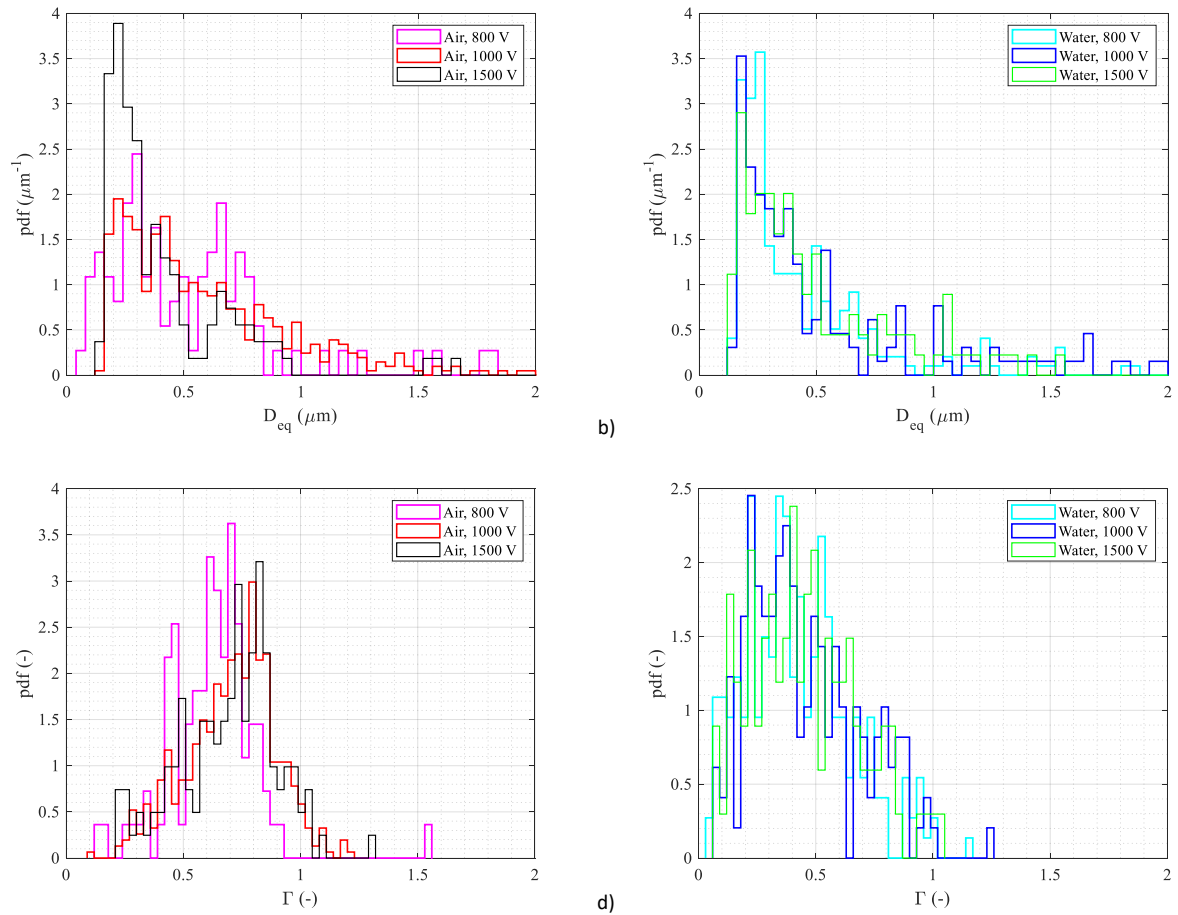


Figure 8. Equivalent diameter distribution for a) air- and b) water-based explosions, and circularity distribution for c) air- and d) water-based explosions. The bin width is 40 nm.

Figure 9 highlights that by utilizing a higher input energy, we eventually obtain a larger fraction of smaller particles in the case of air as medium in which the explosion takes place. We notice that the distribution obtained in the case of air and 800 V has a double-peak behavior, hence the use of lognormal model has some major reliability concerns, and Figure 9 shows a not monotone behavior. In the case of water as medium, an increasing E causes the average equivalent diameter to grow, and this is the opposite of the attended result.

It is worth noting that the in-water explosions create clusters and nanoparticles with lower circularity (Figure 8). On one hand, this can trivially indicate that the nanoparticles have a larger D_{eq} and their shape is less regular due to the interaction with the surrounding media; on the other hand, the same result could be obtained for a larger aggregation of smaller particles, thus resulting in larger and less regular clusters. Indeed, with the used magnification and SEM detector, we cannot distinguish the

forementioned occurrences. A preliminary analysis on the same samples at larger magnification (i.e., 100k) showed that the bigger particles detected with the method described in this study are indeed larger clusters of smaller particles, as showed in Figure 10.

It appears that the impurities contained in the used water could have promoted the aggregation of nanoparticles, thus introducing a bias in the estimation of the equivalent diameter distribution.

Table 1. Parameters associated with the obtained data.

Parameter	Air			Water		
$E(J)$	259 ± 4	391 ± 3	871 ± 8	249 ± 5	386 ± 1	868 ± 7
$D_{eq}^*(nm)$	458	484	376	369	372	395
$D_{eq}(nm)$	446 ± 58	481 ± 20	379 ± 34	370 ± 24	373 ± 28	395 ± 38
$C(250 nm)$	25 %	13 %	28 %	28 %	27 %	26 %
$\Gamma (-)$	0.62 ± 0.04	0.70 ± 0.02	0.70 ± 0.03	0.42 ± 0.03	0.45 ± 0.03	0.44 ± 0.04

[†]Uncertainties of the mean of the equivalent diameter and of Γ are expanded with $k = 2$.

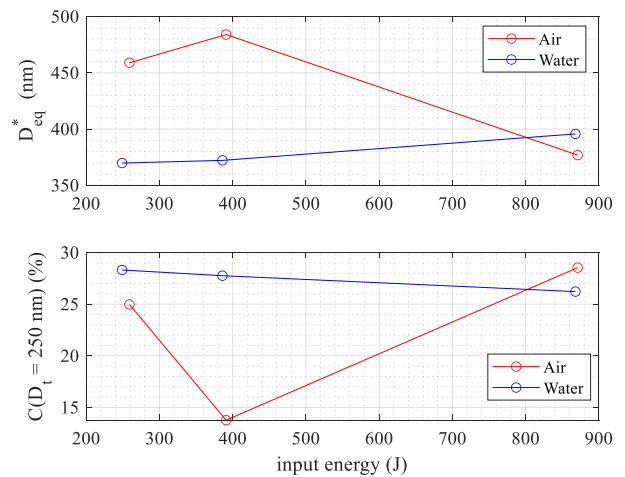


Figure 9. D_{eq}^* (upper) and $C(250 nm)$ (lower) calculated utilizing a model based on a lognormal distribution of the particle size.

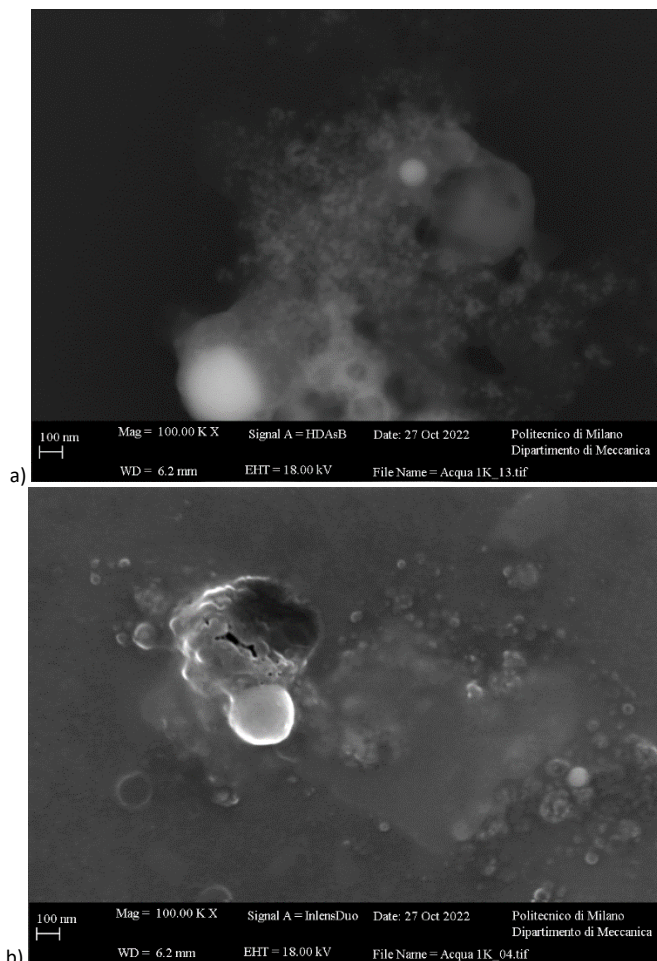


Figure 10. Preliminary picture at 100k magnification of water-based explosion and 1 kV initial voltage.

Therefore, a deeper study based on back-scattered electrons and Energy Dispersive X-ray Spectroscopy is mandatory to shed light on the product morphology and chemistry as a function of the input energy and the medium in which the explosion takes place.

According to the present finding, further investigation is required on a wider range of operating conditions with the purpose of developing a phenomenological model of the process. Moreover, the development of a novel and comprehensive method for the analysis of the nanoparticles is crucial to achieve satisfactory reliability of the results.

5. CONCLUSIONS

In the present work, we developed a setup to produce nanopowder from electrically conductive wires via wire explosion technique. In particular, we produced powder from copper wires with nanometer scale diameter by using current densities in the order of $10^9 - 10^{10}$ A/m², and different explosion atmospheres (i.e., water and air). We collected powder's samples on silicon surfaces, and we further analyze the products morphology by means of a SEM. We used an image analysis tool based on Matlab software to analyze the samples, by measuring the equivalent diameter and circularity distribution of the powder. By using air as medium in which the explosion takes place, it turns out that the dimensional distribution of the nanoparticles is shifted towards smaller equivalent diameter when higher input energy is used. However, the data obtained

from the in-water experiments show an inverted trend. A deeper analysis showed that the larger detected clusters are indeed large aggregation of small particles. Therefore, we infer that the higher input energy contributes to significantly decrease the equivalent diameter of the products, but significant efforts are still required to shed light to this occurrence.

REFERENCES

- [1] Q. Sun, T. Liu, T. Wen, J. Yu, Optimization of particle size, dispersity, and conductivity of 8 mol% Y₂O₃ doped tetragonal zirconia polycrystalline nanopowder prepared by modified sol-gel method via activated carbon absorption, *J Eur Ceram Soc*, 2022. DOI: [10.1016/j.jeurceramsoc.2022.06.017](https://doi.org/10.1016/j.jeurceramsoc.2022.06.017)
- [2] M. Turker, Effect of production parameters on the structure and morphology of Ag nanopowders produced by inert gas condensation, *Materials Science and Engineering: A*, vol. 367, no. 1, 2004, pp. 74–81. DOI: [10.1016/j.msea.2003.10.290](https://doi.org/10.1016/j.msea.2003.10.290)
- [3] J. S. Alzahrani, M. Hessien, Z. A. Alrowaili, I. Kebaili, I. O. Olarinoye, H. Arslan, M. S. Al-Buriahi, Fabrication and characterization of La₂O₃–Fe₂O₃–Bi₂O₃ nanopowders: Effects of La₂O₃ addition on structure, optical, and radiation-absorption properties, *Ceram Int*, vol. 48, no. 16, 2022, pp. 22943–22952. DOI: [10.1016/j.ceramint.2022.04.255](https://doi.org/10.1016/j.ceramint.2022.04.255)
- [4] K. Sonoda, M. Teirikangas, J. Juuti, Y. Moriya, H. Jantunen, Effect of surface modification on dielectric and magnetic properties of metal powder/polymer nanocomposites, *J Magn Magn Mater*, vol. 323, no. 17, 2011, pp. 2281–2286. DOI: [10.1016/j.jmmm.2011.04.007](https://doi.org/10.1016/j.jmmm.2011.04.007)
- [5] M. Palencia, J. A. Ramírez-Rincón, D. F. Restrepo-Holguín, 9 - Polymer-metal oxide composite as sensors, in *Renewable Polymers and Polymer-Metal Oxide Composites*, S. Haider and A. Haider, Eds. Elsevier, 2022, pp. 283–306. DOI: [10.1016/B978-0-323-85155-8.00003-0](https://doi.org/10.1016/B978-0-323-85155-8.00003-0)
- [6] Libing Wang, Wei Ma, Liguang Xu, Wei Chen, Yingyue Zhu, Chuanlai Xu, N. A. Kotov, Nanoparticle-based environmental sensors, *Materials Science and Engineering: R: Reports*, vol. 70, no. 3–6, Nov. 2010, pp. 265–274. DOI: [10.1016/j.mser.2010.06.012](https://doi.org/10.1016/j.mser.2010.06.012)
- [7] V. Sharma, S. Choudhary, P. Mankotia, A. Kumari, K. Sharma, R. Sehgal, V. Kumar, Nanoparticles as fingerprint sensors, *TrAC Trends in Analytical Chemistry*, vol. 143, Oct. 2021, p. 116378. DOI: [10.1016/j.trac.2021.116378](https://doi.org/10.1016/j.trac.2021.116378)
- [8] Vikas, P. Saccomandi, Antimonene-Coated Uniform-Waist Tapered Fiber Optic Surface Plasmon Resonance Biosensor for the Detection of Cancerous Cells: Design and Optimization,” *ACS Omega*, vol. 8, no. 5, Feb. 2023, pp. 4627–4638. DOI: [10.1021/acsomega.2c06037](https://doi.org/10.1021/acsomega.2c06037)
- [9] Kookjin Heo, Jehong Im, Seokhun Kim, Chang-Kee Lee, Duck Rye Chang, Jaekook Kim, Jong-Won Lee, Jinsub Lim, Effect of nanoparticles in cathode materials for flexible Li-ion batteries, *Journal of Industrial and Engineering Chemistry*, vol. 81, 2020, pp. 278–286. DOI: [10.1016/j.jiec.2019.09.015](https://doi.org/10.1016/j.jiec.2019.09.015)
- [10] T. Hirose, T. Omatsu, M. Sugiyama, S. Inasawa, S. Koda, Au-nano-particles production by pico-second ultra-violet laser deposition in Au-ion doped PMMA film, *Chem Phys Lett*, vol. 390, no. 1, pp. 166–169, 2004. DOI: [10.1016/j.cplett.2004.04.011](https://doi.org/10.1016/j.cplett.2004.04.011)
- [11] S. Machmudah, Wahyudiono, Y. Kuwahara, M. Sasaki, M. Goto, Nano-structured particles production using pulsed laser ablation of gold plate in supercritical CO₂, *J Supercrit Fluids*, vol. 60, 2011, pp. 63–68. DOI: [10.1016/j.supflu.2011.04.008](https://doi.org/10.1016/j.supflu.2011.04.008)
- [12] S. Breitung-Faes, A. Kwade, Nano particle production in high-power-density mills, *Chemical Engineering Research and Design*, vol. 86, no. 4, 2008, pp. 390–394. DOI: [10.1016/j.cherd.2007.11.006](https://doi.org/10.1016/j.cherd.2007.11.006)

- [13] S. Ramesh, S. Vetrivel, P. Suresh, V. Kaviarasan, Characterization techniques for nano particles: A practical top down approach to synthesize copper nano particles from copper chips and determination of its effect on planes, *Mater Today Proc*, vol. 33, 2020, pp. 2626–2630.
DOI: [10.1016/j.matpr.2020.01.157](https://doi.org/10.1016/j.matpr.2020.01.157)
- [14] E. A. Glazkova, O. V. Bakina, N. G. Rodkevich, A. A. Mosunov, E. A. Vornakova, V. R. Chzhou, M. I. Lerner, Copper ferrite/copper oxides (I, II) nanoparticles synthesized by electric explosion of wires for high performance photocatalytic and antibacterial applications, *Materials Science and Engineering: B*, vol. 283, 2022, p. 115845.
DOI: [10.1016/j.mseb.2022.115845](https://doi.org/10.1016/j.mseb.2022.115845)
- [15] J. Zhao, Z. Xu, W. Yan, H. Liu, Q. Zhang, Characteristics and Diffusion of Electrical Explosion Plasma of Aluminum Wire in Argon Gas, *IEEE Transactions on Plasma Science*, vol. 45, no. 2, 2017, pp. 185–192.
DOI: [10.1109/TPS.2017.2651032](https://doi.org/10.1109/TPS.2017.2651032)
- [16] V. M. Romanova, G. V. Ivanenkov, A. R. Mingaleev, A. E. Ter-Oganesyan, T. A. Shelkovenko, S. A. Pikuz, Electric explosion of fine wires: Three groups of materials, *Plasma Physics Reports*, vol. 41, no. 8, 2015, pp. 617–636.
DOI: [10.1134/S1063780X15080085](https://doi.org/10.1134/S1063780X15080085)
- [17] F. Lv, P. Liu, H. Qi, J. Liu, R. Sun, W. Wang, The early stage of the thermal pulse explosions of aluminum nanowires under different energy deposition levels, *Comput Mater Sci*, vol. 170, 2019, p. 109142.
DOI: [10.1016/j.commatsci.2019.109142](https://doi.org/10.1016/j.commatsci.2019.109142)
- [18] R. B. Bakshat, S. I. Tkachenko, V. M. Romanova, A. R. Mingaleev, V. I. Oreshkin, A. E. Ter-Oganes'yan, T. A. Khattatov, T. A. Shelkovenko, S. A. Pikuz, Stratification dynamics and the development of electrothermal instability at the wire explosion, *Technical Physics*, vol. 58, no. 8, 2013, pp. 1129–1137.
DOI: [10.1134/S1063784213080021](https://doi.org/10.1134/S1063784213080021)
- [19] B. Liu, D. Wang, Y. Guo, Effect of Circuit Parameters and Environment on Shock Waves Generated by Underwater Electrical Wire Explosion, *IEEE Transactions on Plasma Science*, vol. 45, no. 9, 2017, pp. 2519–2526.
DOI: [10.1109/TPS.2017.2739757](https://doi.org/10.1109/TPS.2017.2739757)
- [20] K. V. Suliz, A. Yu. Kolosov, V. S. Myasnichenko, N. I. Nepsha, N. Yu. Sdobnyakov, A. V. Pervikov, Control of cluster coalescence during formation of bimetallic nanoparticles and nanoalloys obtained via electric explosion of two wires, *Advanced Powder Technology*, vol. 33, no. 3, 2022, p. 103518.
DOI: [10.1016/j.apt.2022.103518](https://doi.org/10.1016/j.apt.2022.103518)
- [21] Yu. A. Kotov, E. I. Azarkevich, A. I. Medvedev, A. M. Murzakaev, V. L. Kuznetsov, O. M. Samatov, T. M. Demina, O. R. Timoshenkova, A. K. Shtoltz, Iron oxide nanopowders prepared by the electroexplosion of wire, *Inorganic Materials*, vol. 43, no. 6, 2007, pp. 633–637.
DOI: [10.1134/S0020168507060143](https://doi.org/10.1134/S0020168507060143)
- [22] X. Gao, C. Xu, H. Yin, X. Wang, Q. Song, P. Chen, Preparation of graphene by electrical explosion of graphite sticks, *Nanoscale*, vol. 9, no. 30, 2017, pp. 10639–10646.
DOI: [10.1039/C7NR01647F](https://doi.org/10.1039/C7NR01647F)
- [23] K. Suliz, A. Miller, K. Ivanov, A. Pervikov, Synthesizing multicomponent AlCrFeCuNi nanoparticles by joint electrical explosion of wires, *Powder Technol*, vol. 404, 2022, p. 117491.
DOI: [10.1016/j.powtec.2022.117491](https://doi.org/10.1016/j.powtec.2022.117491)
- [24] G. Bandini, M. Marracci, G. Caposciutti, B. Tellini, Pulsed-Current Distribution in Electromagnetic Rail Launchers, *IEEE Trans Instrum Meas*, vol. 69, no. 12, 2020, pp. 9381–9388.
DOI: [10.1109/TIM.2020.3006610](https://doi.org/10.1109/TIM.2020.3006610)
- [25] Y. A. Kotov, Electric Explosion of Wires as a Method for Preparation of Nanopowders, *Journal of Nanoparticle Research*, vol. 5, no. 5, 2003, pp. 539–550.
DOI: [10.1023/B:NANO.00000006069.45073.0b](https://doi.org/10.1023/B:NANO.00000006069.45073.0b)
- [26] Mathworks, *Image Processing Toolbox™ User's Guide*, Revised for Version 11.5, 2022.
- [27] C. Peng, J. Wang, N. Zhou, G. Sun, Fabrication of nanopowders by electrical explosion of a copper wire in water, *Current Applied Physics*, vol. 16, no. 3, 2016, pp. 284–287.
DOI: [10.1016/j.cap.2015.12.009](https://doi.org/10.1016/j.cap.2015.12.009)
- [28] Jiangbo Zhang, Xingwen Li, Huantong Shi, Yuhua Zhao, Lei Liang, Wenrong Yan, Fengqi Zhao, Understanding titanium carbide nanoparticle formation by an underwater electrical explosion process through experimental and modeling studies, *Phys Plasmas*, vol. 27, no. 2, Feb. 2020, p. 023510.
DOI: [10.1063/1.5124409](https://doi.org/10.1063/1.5124409)
- [29] L. B. Kiss, J. Söderlund, G. A. Niklasson, C. G. Granqvist, New approach to the origin of lognormal size distributions of nanoparticles, *Nanotechnology*, vol. 10, no. 1, 1999, p. 25.
DOI: [10.1088/0957-4484/10/1/006](https://doi.org/10.1088/0957-4484/10/1/006)
- [30] R. Kissell, J. Poserina, *Advanced Math and Statistics*, in *Optimal Sports Math, Statistics, and Fantasy*, Elsevier, 2017, pp. 103–135.
DOI: [10.1016/B978-0-12-805163-4.00004-9](https://doi.org/10.1016/B978-0-12-805163-4.00004-9)
- [31] M. Borowska, K. Jankowski, Green synthesis of selenium nanoparticles: characterization and application, in *Handbook of Greener Synthesis of Nanomaterials and Compounds*, Elsevier, 2021, pp. 171–190.
DOI: [10.1016/B978-0-12-822446-5.00007-1](https://doi.org/10.1016/B978-0-12-822446-5.00007-1)
- [32] C. H. Cho, S. H. Park, Y. W. Choi, B. G. Kim, Production of nanopowders by wire explosion in liquid media, *Surf Coat Technol*, vol. 201, no. 9, 2007, pp. 4847–4849.
DOI: [10.1016/j.surfcoat.2006.07.032](https://doi.org/10.1016/j.surfcoat.2006.07.032)
- [33] Y. Chen, J. L. Wagner, P. A. Farias, E. P. DeMauro, D. R. Guildenbecher, Galinstan liquid metal breakup and droplet formation in a shock-induced cross-flow, *Int. Journal of Multiphase Flow*, vol. 106, 2018, pp. 147–163.
DOI: [10.1016/j.ijmultiphaseflow.2018.05.015](https://doi.org/10.1016/j.ijmultiphaseflow.2018.05.015)